nature communications

Article

https://doi.org/10.1038/s41467-024-55051-x

Bone Marrow Endothelial Progenitor Cells remodelling facilitates normal hematopoiesis during Acute Myeloid Leukemia Complete Remission

Received: 12 February 2024

Accepted: 27 November 2024

Published online: 30 December 2024

Check for updates

Tong Xing[1,2,3], Li-Juan Hu[1,3], Hong-Yan Zhao[1], Chen-Yuan Li[1], Zhen-Kun Wang[1], Meng-Zhu Shen[1], Zhong-Shi Lyu[1], Jing Wang[1], Yu Wang[1], Hao Jiang[1], Qian Jiang[1], Ying-Jun Chang[1], Xiao-Hui Zhang[1], Yuan Kong[1,4] ✉ & Xiao-Jun Huang[1,2,4] ✉

Although acute myeloid leukemia (AML) affects hematopoietic stem cell (HSC)-supportive microenvironment, it is largely unknown whether leukemia-modified bone marrow (BM) microenvironment can be remodeled to support normal hematopoiesis after complete remission (CR). As a key element of BM microenvironment, endothelial progenitor cells (EPCs) provide a feasible way to investigate BM microenvironment remodeling. Here, we find reduced and dysfunctional BM EPCs in AML patients, characterized by impaired angiogenesis and high ROS levels, could be partially remodeled after CR and improved by N-acetyl-L-cysteine (NAC). Importantly, HSC-supporting ability of BM EPCs is partially recovered, whereas leukemia-supporting ability is decreased in CR patients. Mechanistically, the transcriptome characteristics of leukemia-modified BM EPCs return to near-normal after CR. In a classic AML mouse and chemotherapy model, BM vasculature and normal hematopoiesis are reversed after CR. In summary, we provide further insights into how leukemia-modified BM microenvironment can be remodeled to support normal hematopoiesis after CR, which can be further improved by NAC.

Hematopoiesis is maintained by self-renewing hematopoietic stem cells (HSCs), which reside in the bone marrow (BM) microenvironment[1,2]. Overall, BM endothelial progenitor cells (EPCs), perivascular cells, endosteal cells, and immune cells have been identified as crucial components that regulate HSCs in the BM microenvironment[2–6]. Acute myeloid leukemia (AML) is an aggressive leukemia characterized by the blockage of differentiation and excessive proliferation of leukemia stem cells (LSCs)[7,8]. Leukemia cells can reportedly overwhelm an HSC-supportive microenvironment and potentially modify a normal BM microenvironment into a leukemia-supportive microenvironment[9–11]. As a result, the AML-modified BM microenvironment may outcompete the healthy hematopoiesis microenvironment, leading to anemia and thrombocytopenia in patients with de novo AML[12–14].

Myeloablative therapies, including chemotherapy and allogeneic hematopoietic stem cell transplantation (allo-HSCT), are commonly utilized in patients with AML[7,15,16]. Many patients who undergo chemotherapy suffer poor hematopoiesis recovery, characterized by prolonged cytopenia and increased risk of bleeding, infection, and

[1]Peking University People's Hospital, Peking University Institute of Hematology, National Clinical Research Center for Hematologic Disease, Beijing Key Laboratory of Hematopoietic Stem Cell Transplantation, Collaborative Innovation Center of Hematology, Peking University, Beijing, China. [2]Peking-Tsinghua Center for Life Sciences, Academy for Advanced Interdisciplinary Studies, Peking University, Beijing, China. [3]These authors contributed equally: Tong Xing, Li-Juan Hu. [4]These authors jointly supervised this work: Yuan Kong, Xiao-Jun Huang. ✉e-mail: successky@163.com; huangxiaojun@bjmu.edu.cn

https://doi.org/10.1038/s41467-024-55051-x

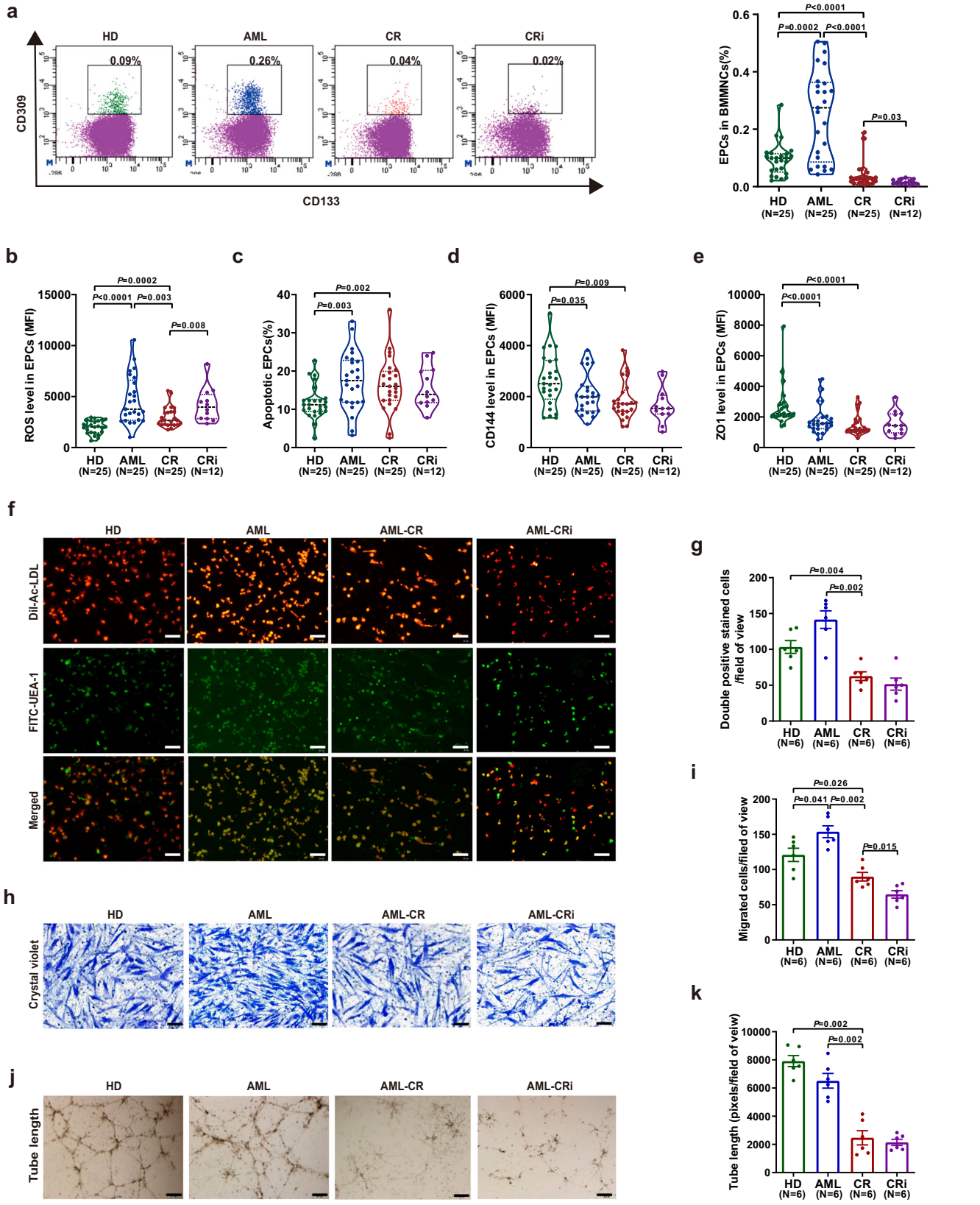

delayed systemic therapy, which imposes a major economic burden on both the healthcare system and patients[17,18]. Alternatively, when AML patients achieve complete remission (CR), HSCs can rapidly amplify and promote normal hematopoietic reconstitution, whereas leukemia cells lose their priority. These clinical phenomena indicate that the BM microenvironment may be quantitatively and functionally different in patients with de novo AML (AML patients) and in AML patients who achieve CR (CR patients). Therefore, we speculate that the remodeled BM microenvironment after CR may enable normal hematopoiesis to dominate, thereby suppressing leukemia cells in AML patients. Moreover, there are some other potential causes of failure to achieve normal hematopoiesis following successful anti-leukemia therapy. These

Fig. 1 | The number and functions of bone marrow (BM) endothelial progenitor cells (EPCs) from complete remission (CR) patients were partially remodeled to those of normal BM EPCs compared to de novo acute myeloid leukemia (AML) patients. a, left The EPC phenotype was characterized by $CD34^+CD309^+CD133^+$, as determined by flow cytometry. **a, right** The percentage of BM EPCs in precultivated BM mononuclear cells (BMMNCs) was analyzed. **b** The ROS levels, **c** apoptosis ratio, **d** CD144 level and **e** ZO1 level in precultivated BM EPCs from HDs (N = 25), patients with AML (N = 25), CR (N = 25) and CRi (N = 12). **b**–**e** Twenty-five paired samples from each of the groups (N = 25 per group, n = 1 per sample) were collected on different days, with one sample per group analyzed together on the same day. CRi group(N = 12, n = 1) was performed during the revision. **f** Representative images (scale bar = 200 μm) of typical cultured BM EPCs collected on day 7 of culture were characterized by double-positive staining (merged in yellow) with DiI-Ac-LDL (red) and FITC-labeled Ulex Europaeus Agglutinin-I (FITC-UEA-I) (green) (original magnification, 10×). **g** Quantification of double-positive EPCs/field of view (merged in yellow) stained with DiI-Ac-LDL (red) and FITC-UEA I (green) on day 7 of culture (original magnification, 10×) **h** After 7 days of culture, BM EPCs were cultured in a transwell chamber for 24 h, fixed and stained with crystal violet. Representative images (scale bar = 200 μm) and **i** the number of migrated cells per field of view on the bottom surface of the membrane (original magnification, 10×) Three power fields were randomly counted, and the values were averaged for each sample. **j** Representative images (scale bar = 200 μm) of tube formation (pixels of tubes per field of view) and **k** quantification of the tube length of BM EPCs after 7 days of culture (original magnification, 10×). **f**–**k** Six paired samples from each of the groups (N = 6 per group, n = 3 per sample) were collected on different days, with one sample per group analyzed together on the same day. N represents biological replicates; n represents technical replicates. Statistical analyses were performed using the Mann–Whitney U test. The data are presented as the means ± SEMs. The statistical tests were two-sided and no adjustments were made for multiple comparisons. Source data are provided as a Source Data file.

include HSC dysfunction, inhibition of production of downstream hematopoietic cells by impeding differentiation at the HSC–progenitor transition, immune-mediated hematopoietic failure, clonal hematopoiesis, and co-existing myelodysplastic neoplasms[19,20]. Given the absence of relevant reports, it is highly important to explore whether the BM microenvironment could be remodeled after CR and how to improve the remodeling process to promote normal hematopoiesis in AML patients.

Many studies have revealed that BM EPCs play an essential role in regulating hematopoiesis during homeostasis[3,5,21]. In contrast, dysfunctional EPCs, which are characterized by increased levels of reactive oxygen species (ROS) and apoptosis, impaired angiogenesis, and HSC-supporting abilities, are involved in the pathogenesis of several human diseases, such as poor hematopoietic function after allo-HSCT[22,23], corticosteroid-resistant immune thrombocytopenia[24], and aplastic anemia[25]. Integrated data from in vitro studies and prospective clinical trials provided direct evidence that N-acetyl-L-cysteine (NAC, a ROS scavenging agent) effectively promoted HSC reconstitution by improving BM EPC function in patients with acute leukemia after allo-HSCT[22,23,26,27]. In AML, the BM microenvironment is modified into a highly vascularized malignant BM microenvironment, which enhances LSC renewal but inhibits normal HSCs[28,29]. As a key element of the BM microenvironment, BM EPCs provide a feasible way to investigate the functional remodeling of the BM microenvironment, especially the ability of BM EPCs to support HSCs or LSCs, in de novo AML patients and CR patients after chemotherapy[14,28,30,31]. Therefore, a comprehensive understanding of BM EPCs may lead to the identification of candidate interventions that could reverse the AML-modified BM microenvironment to normalize it and provide a potential pathogenesis-oriented therapeutic strategy to further promote healthy hematopoiesis in CR patients.

In this work, the functions and transcriptional characteristics of BM EPCs are examined, and their ability to support HSCs or leukemia cells are compared between patients with de novo AML and in CR. Using in vitro and in vivo studies, we investigate how to improve the BM EPC remodeling process in CR patients to facilitate normal hematopoiesis recovery without affecting leukemia relapse and their underlying mechanisms. Our aim is to provide further insights into how the leukemia-modified BM microenvironment could be remodeled from supporting leukemia at diagnosis to supporting normal hematopoiesis after CR, which may improve the current therapeutic paradigms for AML patients.

Results

The functions of BM EPCs in AML patients after achieving CR (CR patients) were reversed to nearly normal compared to those in de novo AML patients (AML patients)

To compare the quantity and function of BM EPCs from CR patients (CR EPC), from CR patients with incomplete blood count recovery (CRi EPC), from de novo AML patients (AML EPC), and from HDs (HD EPC), the percentage, ROS level, apoptosis ratio, permeability of BM EPCs, tube formation and migration abilities of BM EPCs were investigated. The ages of HDs (47.3 years, range 30-59), CR patients (45 years, range 30-67), and AML patients (43.6 years, range 28-68) were not significantly different. The percentage of CR EPCs was significantly lower (Fig. 1a; 0.04% ± 0.01% vs. 0.26% ± 0.03%, $P < 0.0001$) and accompanied by decreased ROS levels (Fig. 1b; 2984 ± 197 vs. 4675 ± 470, $P = 0.003$) than that of AML EPCs. The percentage of CRi EPCs was lower than CR EPCs (Fig. 1a; 0.02% ± 0.003% vs. 0.04% ± 0.01%, $P = 0.03$), whereas increased ROS levels in CRi EPCs than CR EPCs (Fig. 1b; 4191 ± 478 vs.2984 ± 197, $P = 0.008$). Compared with HD EPCs, reduced percentage (Fig. 1a; 0.04% ± 0.01% vs. 0.09% ± 0.01%, $P < 0.0001$), whereas higher levels of ROS (Fig. 1b, 2984 ± 197 vs. 2003 ± 129; $P = 0.0002$) and apoptosis (Fig. 1c, 16.4% ± 1.4% vs. 11.8% ± 0.9%; $P = 0.002$) were found in CR EPCs. The gating strategy for the apoptosis of EPCs was shown in Fig. S1a. CR EPCs showed greater permeability than HD EPCs, as characterized by decreased levels of CD144 (Fig. 1d; 1867 ± 150 vs. 2630 ± 207; $P = 0.009$) and ZO1 (Fig. 1e; 1490 ± 140 vs. 2688 ± 271; $P < 0.0001$).

CR patients had fewer double-positive stained BM EPCs (Fig. 1f, g; 63 ± 6 vs. 142 ± 12; $P = 0.002$), significantly fewer migrated cells (Fig. 1h; i, 90 ± 6 vs. 154 ± 8; $P = 0.002$), and less tube formation ability (Fig. 1j; k, 2468 ± 503 vs. 6516 ± 519; $P = 0.002$) than AML patients. Compared with CR patients, CRi patients exhibited decreased migration ability of BM EPCs (Fig. 1h; i, 65 ± 5 vs. 90 ± 6; $P = 0.015$). Compared with HD, CR patients exhibited fewer double-positive stained BM EPCs (Fig. 1f; 1 g, 63 ± 6 vs. 103 ± 9; $P = 0.004$), decreased migration (Fig. 1h; i, 90 ± 6 vs. 121 ± 9; $P = 0.026$) and tube formation (Fig. 1j; k, 2468 ± 503 vs. 7914 ± 393; $P = 0.002$). Our data indicated that the dysfunctional BM EPCs in AML may drive delayed count recovery following induction therapy. However, CR EPCs still exhibited higher levels of ROS, apoptosis and permeability than did HD EPCs, indicating the necessity of further improving the functions of CR EPCs.

The hematopoiesis-supporting ability of CR EPCs was remodeled to become more similar to that of normal BM EPCs

To evaluate the differences in the hematopoiesis-supporting ability and leukemia-supporting ability of BM EPCs, we evaluated the functions of HSCs and leukemia cells after coculture with BM-EPCs (Fig. 2a). Compared with those after coculture with AML EPCs, colony-forming unit erythroid (CFU-E) (Fig. 2b) and burst-forming unit erythroid (BFU-E)(Fig. 2b) plating efficiencies of HSCs were significantly higher, HSCs exhibited decreased ROS levels (Fig. 2c) but increased apoptosis ratios (Fig. 2d) after coculture with CR EPCs. The percentages of 5-ethynyl-20-deoxyuridine (EdU)-positive leukemia $CD34^+$ cells (Fig. 2e; 1.0 ± 0.1-fold vs. 1.6 ± 0.2-fold; $P = 0.04$), KG-1 cells and HL-60 cells were lower, but the apoptotic rates of leukemia $CD34^+$ cells were notably greater (Fig. 2f; 1.4 ± 0.2-fold vs. 0.9 ± 0.1-fold; $P = 0.026$), and the apoptotic

https://doi.org/10.1038/s41467-024-55051-x

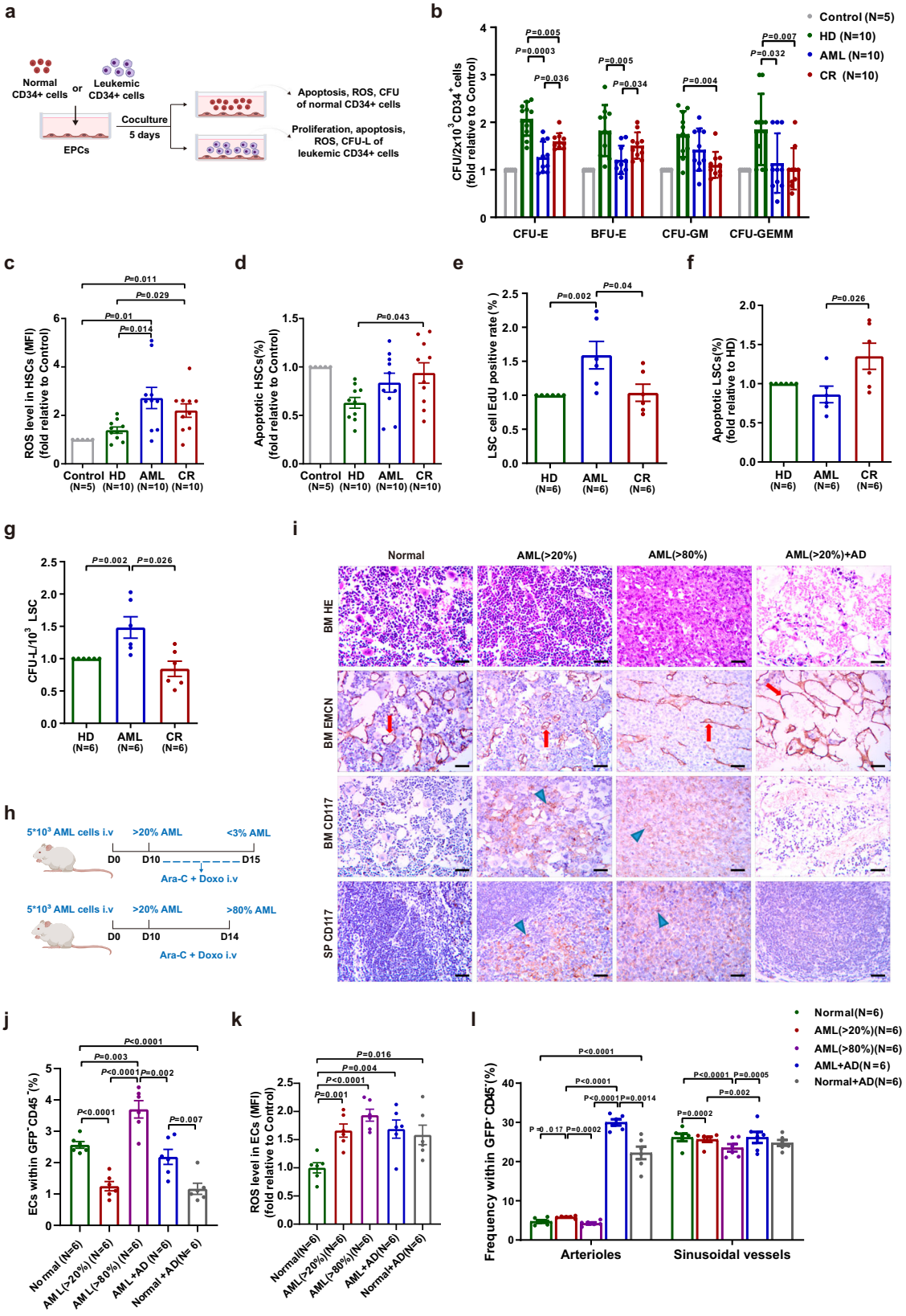

rates of KG-1 and HL-60 cells were higher in CR group than in AML group (Fig. 2e, f and Fig. S1). Gating strategies for EdU-positive of leukemia cells, the apoptosis of leukemia cells and the ROS of leukemia cells were shown in Fig. S1b–d. The leukemia colony-forming unit (CFU-L) plating efficiencies of leukemia $CD34^+$ cells (Fig. 2g; 0.8 ± 0.1-fold vs. 1.5 ± 0.2-fold; $P = 0.026$), KG-1 and HL-60 cells in CR group were markedly lower (Fig. S1). These data demonstrated that the ability of CR EPCs to support HSCs was partially restored, whereas their leukemia-supporting ability was decreased compared to that of AML EPCs.

HSCs cocultured with CR EPCs had lower colony-forming unit (CFU) plating efficiencies (Fig. 2b), than did those cocultured with HD

Fig. 2 | The hematopoiesis-supporting ability of BM EPCs from CR patients was remodeled compared to that from AML patients, and BM vasculature and EC function were remodeled in AML mice after chemotherapy. a Schematic diagram of the study design for the process of coculturing BM EPCs with HSCs or leukemic CD34$^+$ cells. **b** The CFU plating efficiency of HSCs, as determined by colony-forming unit (CFU), burst-forming unit erythroid (BFU-E), colony-forming unit granulocyte/macrophage (CFU-GM), and colony-forming unit granulocyte, erythroid, macrophage and megakaryocyte (CFU-GEMM), after coculture with BM EPCs from HDs, patients with AML and CR (N = 10 per group, n = 3 per sample). Quantification of **c** ROS levels and **d** the apoptotic ratio of HSCs after coculture with BM EPCs are shown (N = 10 per group, n = 1 per sample). Quantification of **e** the percentages of EdU-positive **f** apoptosis ratio, **g** leukemia colony-forming units (CFU-L) of leukemic CD34$^+$ cells after coculture with BM EPCs are shown (N = 6 per group, n = 1 per sample). **b**–**g** The paired samples from each of the groups were collected on different days, with one sample per group analyzed together on the same day. **h** Schematic diagram of the design of the study of AML mouse model. **i** Femoral sections stained with HE, an anti-endomucin (EMCN) antibody (red arrow) and a CD117 antibody (blue arrow). Representative images showing increased and structurally disordered vessels in the AML mice at primary disease stages (> 20% BM infiltration, AML (> 20%)), compressed vessels at advanced disease stage (> 80% BM infiltration, AML (> 80%)) and dilated vessels after chemotherapy (AML + AD mice) compared to those in the normal group (Normal). The AML + AD group showed completely cleared CD117$^+$ cells (brown) in the BM and spleen (SP) (scale bar=10 μm). **j** The frequency of CD31$^+$VE-cadherin$^+$ ECs within the CD45$^-$Ter119$^-$ BM cells from mice given the indicated treatments was analyzed by flow cytometry. **k** Quantification of intracellular ROS levels in BM ECs among all the mouse groups. **l** Quantification of subtypes BM ECs among all the mouse groups. **j**–**l** The paired samples from each of the murine groups (N = 6 per group, n = 1 per sample) were collected and analyzed at indicated days. N represents biological replicates; n represents technical replicates. Statistical analyses were performed using the Mann–Whitney U test and unpaired t test. The data are presented as the means ± SEMs. The statistical tests were two-sided and no adjustments were made for multiple comparisons. Source data are provided as a Source Data file.

EPCs. ROS levels (Fig. 2c; 2.2 ± 0.3-fold vs. 1.4 ± 0.1-fold; P = 0.029) and apoptosis rates (Fig. 2d; 0.9 ± 0.1-fold vs. 0.6 ± 0.1-fold; P = 0.043) of HSCs in CR group were markedly greater than HD group. The percentage of apoptotic cells in KG-1 (Fig. S1f) or HL-60 cells (Fig. S1i) was notably greater in CR group than in HD group. Together, these findings suggested that the hematopoiesis-supporting ability of CR EPCs was remodeled to become more similar to that of normal BM EPCs, which benefited normal hematopoiesis recovery, but still needs to be improved.

BM vasculature and EC function were remodeled after CR in a classic AML mouse model

To provide a detailed picture of the role of BM ECs in AML and after CR, we studied the morphology and functions of BM ECs in a AML-ETO-induced AML mouse model (Fig. 2h). The AML mice with greater than 20% infiltration in BM (AML (> 20%)) had a high WBC count, anemia, thrombocytopenia, splenomegaly and suppression of erythropoiesis in femur on day 10 (Figs. 2i, j and Fig. S2a–d). All the above-mentioned symptoms were aggravated when the mice had greater than 80% infiltration of BM (AML (> 80%)) on day 15. After chemotherapy in AML mice (AML + AD mice), AML cells in BM were below 1%, and all AML-related manifestations were gone.

To quantify BM blood vessels in AML mice before and after chemotherapy, BM ECs were detected by flow cytometry (Fig. S2e) and visualized by immunohistochemistry (IHC) (Fig. 2i). Most vessels in AML mice were narrower than those in normal mice (Fig. 2i). After 5 days of chemotherapy, the vessels of AML mice were extensively decompressed but dilated (Fig. 2i), and the number of BM ECs (Fig. 2j; 2.2 ± 0.2% vs. 3.7 ± 0.3%; P = 0.002) was markedly lower than that in AML mice (> 80%). The quantity of post-chemo normal ECs in AD group was lower than those in AML + AD group on day 1 after the end of chemotherapy (Fig. 2j; 1.2 ± 0.2% vs. 2.2 ± 0.2%; P = 0.007). The ROS level of BM ECs in AML + AD mice was decreased than AML mice (> 80%), but was still notably greater than that in control group (Fig. 2k; 1.7 ± 0.2-fold vs. 1.0 ± 0.1-fold; P = 0.004). In addition, we found a marked increment in the number of arteriolar ECs (CD31$^+$Sca1^{high}) (Fig. 2l; 5.8 ± 0.1% vs. 4.7 ± 0.4%; P = 0.017), accompanied by a notable decline in sinusoidal ECs (CD31$^+$Sca1^{low}) (Fig. 2l; 19.7 ± 0.7% vs.26.2 ± 0.9%; P = 0.0002) from AML mice (> 20%) compared with normal mice. Gating strategies for quantification and subtypes of BM ECs, HSPCs and myeloid cells were shown in Fig. S2f–h.Together, these results showed that AML is associated with a structurally and functionally abnormal vasculature in BM, and these abnormalities could be modified after chemotherapy, which may be one of the reasons for the promotion of normal hematopoietic reconstitution in AML + AD mice.

The BM EPC functions of CR EPCs were further improved by NAC in vitro

Due to the high ROS level in BM EPCs, we next examined whether NAC could improve the function of BM EPCs from CR patients. After NAC treatment, ROS levels (Fig. 3a; 5814 ± 684 vs. 8629 ± 808; P = 0.012) and apoptosis rate (Fig. 3b; 14.9% ± 0.8% vs. 22.9% ± 2.0%; P = 0.005) of CR EPCs were markedly decreased. The permeability of CR EPCs was decreased by NAC treatment, as indicated by elevated CD144 (Fig. 3c; 3289 ± 159 vs. 2697 ± 122; P = 0.023) and ZO1 (Fig. 3d; 3009 ± 167 vs. 2176 ± 154; P = 0.005). Moreover, the levels of ROS, CD144 and ZO1 did not differ significantly between NAC-treated CR EPCs and HD EPCs. The numbers of double-positive cells (Fig. 3e, f; 81 ± 6 vs. 66 ± 6; P = 0.01), migrated cells (Fig. 3g, h; 114 ± 9 vs. 91 ± 5; P = 0.008) and tube formation ability (Fig. 3i, j; 3928 ± 821 vs. 2142 ± 496; P = 0.004) were greater in NAC treated CR EPCs than untreated CR EPCs. These findings suggested that NAC could further improve the functions of CR EPCs, making them more like normal BM EPCs.

To investigate whether NAC could improve the ability of BM EPCs to support normal or malignant hematopoiesis, direct-contact coculture of HSCs (Fig. 3k–m), leukemic CD34$^+$ cells (from newly diagnosed AML patients), KG-1 cells, or HL-60 cells (Fig. S3) were performed. NAC improved the impaired HSC-supporting ability of CR EPCs, as demonstrated by decreased ROS levels (Fig. 3k; 1.8 ± 0.2-fold vs. 2.4 ± 0.3-fold; P = 0.011) and decreased apoptosis ratios (Fig. 3l; 0.6% ± 0.1% vs. 0.9% ± 0.1%, P = 0.017) of CD34$^+$ cells. BFU-E (1.5 ± 0.1-fold vs. 1.2 ± 0.1-fold; P = 0.045) and colony-forming unit granulocyte/macrophage (CFU-GM) (1.6 ± 0.1-fold vs. 1.2 ± 0.1-fold; P = 0.026) efficiencies were also significantly elevated. Notably, NAC treatment did not affect the ability of CR EPCs to support leukemic CD34$^+$ cells.

NAC promoted hematopoiesis reconstitution by improving BM ECs numbers after CR in AML mice

To examine the effect of NAC on improving BM ECs in vivo, NAC was administered to AML mice after CR and hematopoiesis and BM microenvironment were detected in mice that treated with NAC (CR + NAC group) or not (CR group) on day 10 after the end of chemotherapy (Fig. S4). After NAC therapy, there were no differences in splenomegaly or suppression of erythropoiesis in the femurs of AML mice that achieved CR between CR + NAC group or CR group. Undifferentiated blast infiltration in BM were observed between the two groups (Fig. 4a, b). These results indicated that NAC did not affect leukemia cells after CR in AML mice.

For normal hematopoiesis, PLT count (Fig. 4c; 3172 ± 168 vs. 2628 ± 128; P = 0.03), the ratio of HSPCs (Fig. 4d; 105.3 ± 10.0 vs. 71.4 ± 8.1; P = 0.025) and myeloid cells (Fig. 4e; 70.2% ± 0.8% vs. 60.2% ± 3.4%; P = 0.017) in BM were significantly increased in CR + NAC

https://doi.org/10.1038/s41467-024-55051-x

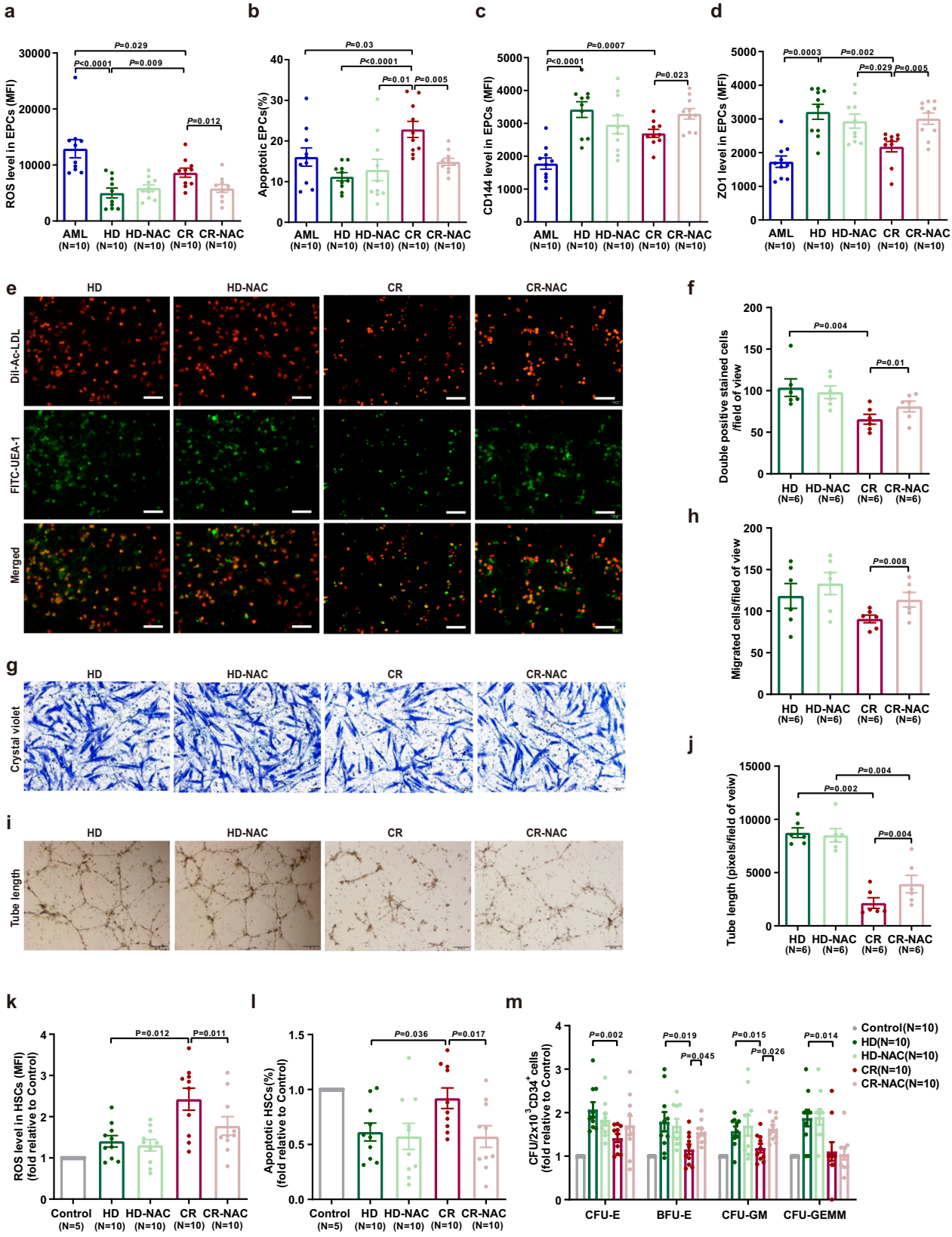

group compared to CR group. Significantly increased BM ECs (Fig. 4f; 3.0 ± 0.4% vs. 1.4 ± 0.2%; $P = 0.003$), decreased ROS levels (Fig. 4g) and restored BM vessel structures (Fig. 4a, h) were observed in CR + NAC group. These results suggested that NAC may promote normal hematopoiesis in AML mice after CR by improving the functions of BM ECs.

Remodeled molecular signatures in CR EPCs

RNA sequencing (RNA-seq) results of unsupervised hierarchical clustering (Fig. 4i) and principal component analysis (PCA) (Fig. 4j) showed heterogeneity in the expression profiles of CR EPCs, AML EPCs and HD EPCs. Notably, the transcriptome characteristics of CR EPCs were more similar to those of HD EPCs but not to those of AML EPCs, indicating

Fig. 3 | The functions and hematopoietic support capacity of BM EPCs from CR patients were further enhanced by NAC in vitro. a ROS levels in cultivated AML EPCs and CR EPCs demonstrated a decrease after NAC treatment. **b** The apoptosis ratio was lower in CR EPCs treated with NAC, indicating improved cell survival. **c** CD144 expression, a key marker for EPCs, was significantly elevated in CR EPCs following NAC exposure. **d** ZO-1 expression, an indicator of cellular integrity, showed an improvement in CR EPCs with NAC. **a**–**d** Ten paired samples from each of the groups (N = 10 per group, $n = 1$ per sample) were collected on different days, with one sample per group analyzed together on the same day. **e** BM EPCs were characterized by double staining with DiI-Ac-LDL(red) and FITC-UEA-1(green), as seen in the merged yellow signal. **f** On Day 7 of culture, the number of double-positive EPCs per field of view was quantified using DiI-Ac-LDL and FITC-UEA-1 staining. **g** Representative images depicted the migration of BM EPCs, with NAC-treated CR EPCs showing increased migration. **h** Quantification of migrated EPCs confirmed this observation. **i** BM EPCs formed tube-like structures, and **j** the tube formation assay revealed a higher number of tubes per field of view in the NAC-treated group. **e**–**j** Six paired samples from each of the groups (N = 6 per group, $n = 3$ per sample) were collected on different days, with one sample per group analyzed together on the same day. **k** ROS levels in HSCs cocultured with CR EPCs were reduced after NAC intervention. **l** The apoptosis rate of HSCs was lower in the presence of NAC-treated CR EPCs. **k, l** Ten paired samples from each of the groups (N = 10 per group, $n = 1$ per sample) were collected on different days, with one sample per group analyzed together on the same day. **m** The colony-forming unit(CFU) plating efficiency of HSCs(from HDs) was significantly enhanced after coculture with NAC-boosted CR EPCs (N = 10 per group, $n = 3$ per sample). All scale bars represent 200 μm, with an original magnification of 10×. N represents biological replicates; n represents technical replicates. Statistical analyses were conducted using paired *t*-tests. The data are presented as the means ± SEMs. The statistical tests were two-sided and no adjustments were made for multiple comparisons. Source data are provided as a Source Data file.

that the molecular signature of CR EPCs was remodeled and was more similar to that of normal BM EPCs.

A total of 1118 genes were upregulated, and 772 genes were downregulated in CR EPCs compared to HD EPCs (Fig. 4k). Gene set enrichment analysis (GSEA) revealed that the blood vessel remodeling pathway (Fig. 4l) and hematopoietic cell lineage pathway (Fig. 4m) were enriched. CR EPCs were activated for the expression of genes involved in ROS pathway (Fig. 4n), p53 pathway (Fig. 4o) and apoptosis pathway (Fig. 4p). These results demonstrated altered transcriptome signatures between AML EPCs and CR EPCs.

NAC might improve the function of BM EPCs from CR patients through inhibition of the ROS-p53 pathway

To determine the underlying mechanism of NAC treatment in BM EPCs, we compared the transcriptome characteristics of CR EPCs before and after NAC treatment in vitro. By the PCA analysis, the transcriptome characteristics of CR EPCs before and after NAC treatment were completely different (Fig. 5a). A total of 527 genes were upregulated, and 202 genes were downregulated. After NAC treatment, the ROS pathway (Fig. 5b), P53 pathway (Fig. 5c) and apoptosis pathway (Fig. 5d) were suppressed according to GSEA analysis. The protein levels of phospho-P53 (Fig. 5e; 3751 ± 220 vs. 3011 ± 252; $P = 0.033$), BAX (Fig. 5f; 1754 ± 137 vs. 1290 ± 76; $P = 0.006$) and cleaved-caspase-3(Fig. 5g; 1260 ± 124 vs. 866 ± 73; $P = 0.016$) were notably greater in CR EPCs, but the protein level of BCL2 (Fig. 5h; 687 ± 57 vs. 888 ± 61; $P = 0.021$) was markedly lower in CR EPCs than in HD EPCs by flow cytometry. The protein levels of phospho-P53, PUMA, BAX and cleaved-caspase-3 were increased but BCL-2 was decreased in CR EPCs compared to those in HD EPCs, and these changes were alleviated by NAC (Fig. 5i). Taken together, our data indicated that NAC might improve the function of CR EPCs by inhibiting the ROS-p53 pathway.

Discussion

Our in vitro and in vivo data demonstrated that AML-modified BM EPCs could be partially remodeled to support normal hematopoiesis after CR. Moreover, experiments in a classical AML murine and chemotherapy model confirmed that NAC can further enhance the functions of the remodeled BM EPCs in AML after CR. Although further validation is needed, our data suggest that NAC is a promising therapeutic strategy for promoting normal hematopoiesis recovery in AML after chemotherapy (Fig. 6).

As a crucial component of the BM vascular microenvironment, well-functioning EPCs regulate HSC homeostasis[3,5,21,32]. In pathogenic conditions, AML-modified BM vasculature architecture and permeability have a reduced capacity to support nonleukemic HSCs, which is correlated with the loss of normal hematopoiesis in mice[28,33]. B Kumar et al. reported that the AML-modified BM microenvironment contributes to the transformation from a normal microenvironment to a leukemia-supportive microenvironment, which outcompetes healthy hematopoiesis[31]. Moreover, a highly vascularized malignant BM microenvironment enhanced LSC renewal but inhibited normal HSC renewal in AML patients[34]. However, the disappointing results of clinical trials of antiangiogenic therapy in AML patients suggested that the vascular alterations in AML-modified BM may be more complex than those in patients with vascular alterations alone[28,35,36], further supporting the importance of remodeling the function of AML BM EPCs to rescue normal hematopoiesis in AML patients. Nevertheless, the available studies evaluating the function of BM EPCs in AML patients after CR, especially the ability of BM EPCs to support HSCs or LSCs, are limited.

The results of the present study demonstrated that AML-modified BM EPCs could be partially remodeled to support normal hematopoiesis after CR. The critical role of functional remodeling of the BM microenvironment was confirmed in AML patients after CR via in vitro studies, followed by in vivo studies using a classic murine AML model. Indeed, our data revealed that BM EPCs were functionally remodeled from supporting AML at diagnosis to supporting normal hematopoiesis after CR. Although the precise mechanisms of BM EPCs regulating on hematopoiesis should be further explored, our data suggested that the remodeling process of BM EPCs may be a key factor for normal hematopoiesis recovery in AML patients.

Elucidation of how to improve impaired BM EPCs to promote normal hematopoiesis is highly important for identifying promising therapeutic approaches. Our previous studies reported that the dysfunctional BM EPCs with high ROS levels contributed to hematopoietic failure, such as aplastic anemia and poor hematopoietic function after allo-HSCT[22–27,37,38]. Increased ROS levels induced dysfunctional BM EPCs with impaired hematopoiesis support ability, leading to defective hematopoiesis[22–27,37,38]. NAC, a widely used clinical drug with few side effects, has been found to ameliorate hematopoietic failure in mice with aplastic anemia and in patients with poor hematopoietic function after allo-HSCT[22–27,37,38]. Here, we found both the reduced and dysfunctional BM EPCs in de novo AML patients and in a classic AML mouse model, characterized by high ROS levels and impaired HSC-supporting ability, could be partially remodeled after CR and were further improved by NAC treatment. Mechanistically, our findings revealed that NAC might enhance the functions of BM EPCs in CR via the ROS-p53 pathway. Therefore, our data indicated that traditional chemotherapy combined with the improvement of BM microenvironment remodeling may be a potential pathogenesis-oriented therapeutic approach for improving the clinical prognosis in patients with AML.

BM ECs are heterogeneous, which can be further subdivided into arteriole/sinusoid ECs. Consistent with the previous reports[33,39], we verified that the increase in BM arteriole ECs whereas the decrease in sinusoid ECs in AML mice. After AD treatment, the level of arterioles increased substantially both in normal AD group and AML + AD group,

https://doi.org/10.1038/s41467-024-55051-x

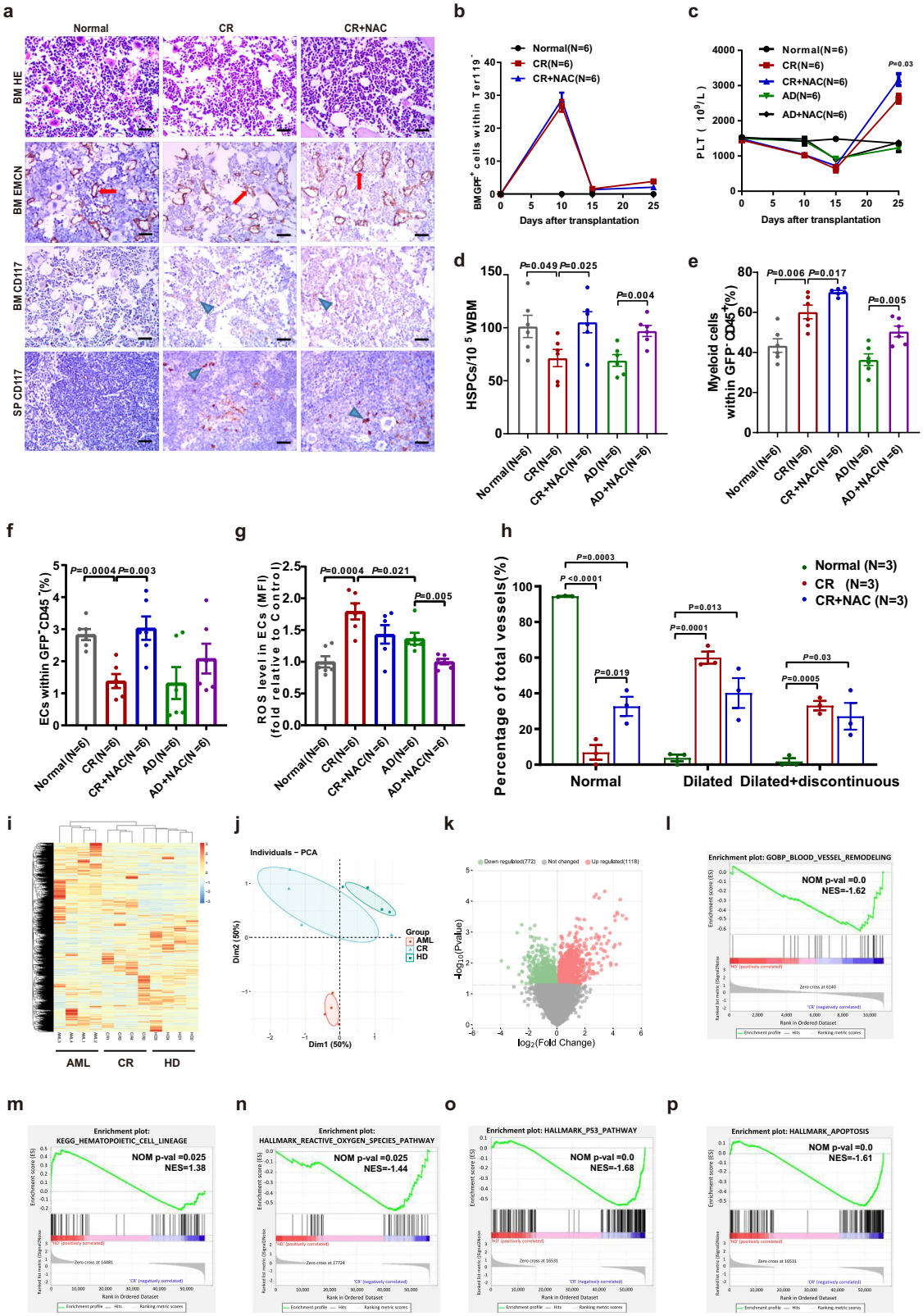

indicating that chemotherapy may act on arteriole/sinusoid ECs differently. Consequently, the current study indicates that it will make sense to divide the arteriole/sinusoid EPC subsets to evaluate the effect of ROS, transcriptomic, the ratios of human arteriole/sinusoid EPC subsets among the HD, AML-CR and AML patient groups, and the murine transcriptome of BM EC subsets, which shed light on valuable directions for the future study.

In this work, our study proposes a concept that AML-modified BM EPCs can be remodeled to support normal hematopoiesis in patients in CR. Although further validation is needed, our preliminary data provide a rationale for further prospective clinical trials that NAC is a promising therapeutic strategy for promoting normal hematopoiesis recovery in AML patients after chemotherapy, which may benefit other cancer patients experiencing myelosuppression in the future.

Fig. 4 | Characteristics of AML mice treated with NAC(CR + NAC) or not(CR) and the normal mice treated with NAC (AD + NAC) or not (AD) and molecular signatures of CR EPCs. a Representative H&E staining images (scale bar=10 μm) of BM sections in murine femurs, representative images of BM ECs in murine femurs stained with anti-EMCN antibody (red arrow) (scale bar = 10 μm) and CD117 antibody (blue arrow) (scale bar = 10 μm), and representative images of SPs stained with CD117 antibody (blue arrow) (scale bar = 10 μm). **b** Ratio of GFP-expressing AML-ETO primary mouse AML cells in BM nucleated cells. **c** Platelet (PLT) counts of all the mice in each group. **d** The frequencies of lineage$^-$cKIT$^+$SCA1$^+$ hematopoietic stem progenitor cells (HSPCs). **e** The frequency of myeloid cells within murine CD45$^+$ BM cells was analyzed by flow cytometry. **f** The frequency of CD31$^+$VE-cadherin$^+$ ECs within the CD45$^-$Ter119$^-$ BM cells from mice given the indicated treatments was analyzed by flow cytometry. **g** Quantification of intracellular ROS levels in BM ECs among all the mouse groups. **b**–**g** Six paired samples from each of the murine groups (N = 6 per group, n = 1 per sample) were collected and analyzed at indicated days. **h** Quantification of damaged BM ECs in murine femurs stained with an anti-EMCN antibody (Three paired samples from each of the murine groups (N = 3 per group, n = 1 per sample) were collected and analyzed at indicated days). **i** Heatmap and hierarchical clustering of RNA-seq data for the 12 libraries using the Euclidean distance. **j** Principal component analysis (PCA) score plot of 12 libraries of HD EPCs (N = 4), AML EPCs (N = 4) and AML CR EPCs (N = 4) at 7 days of culture. **k** Volcano plots of the upregulated genes (red) and downregulated genes (green) of HD EPCs and AML CR-EPCs. Gene set enrichment analysis (GSEA) comparing AML CR-EPCs and HD-EPCs for genes involved in **l** the blood vessel remodeling pathway, **m** the hematopoietic cell lineage pathway, **n** the reactive oxygen species pathway, **o** the P53 pathway and **p** the apoptosis pathway. **i**–**p** Four paired samples from each of the groups (N = 4 per group, n = 1 per sample) were collected on different days, and analyzed on the same day. N represents biological replicates; n represents technical replicates. Statistical analyses were performed using paired t tests. The data are presented as the means ± SEMs. The statistical tests were two-sided and no adjustments were made for multiple comparisons. Source data are provided as a Source Data file.

Methods

The Ethics Committee Review Board of Peking University People's Hospital deemed that this research complies with all relevant ethical regulations (Protocol no. 2020PHB067-01; 2023PHB030-001), and written informed consent was obtained from the subjects in accordance with the Declaration of Helsinki.

Patients and control individuals

In the prospective cohort study, BM specimens from patients with de novo AML (N = 25) (Table S1), CR patients (N = 25), CR patients with incomplete blood count recovery[40](CRi, N = 12), and age-paired healthy donors (HDs, N = 25) collected for allo-HSCT were used as the healthy control group.

CR was defined as BM blasts <5%, absence of circulating blasts or blasts with Auer rods, absence of extramedullary disease, absolute neutrophil count (ANC) ≥ 1.0×10^9/L; platelet ≥100×10^9/L. CRi was defined as all CR criteria except for residual neutropenia <1.0×10^9/L or thrombocytopenia <100×10^9/L[40].

Isolation, cultivation, and characterization of primary BM EPCs

The representative BM EPC phenotype was characterized by CD34$^+$CD309$^+$CD133$^+$ cells. BMMNCs were isolated using lymphocyte separation medium (GE Healthcare, Milwaukee, WI, USA) and then cultured in EGM-2-MV-SingleQuots (Lonza, Walkersville, MD, USA) and 10% fetal bovine serum (FBS, Gibco, MA, USA) for 7 days.

For in vitro NAC treatment, BM EPCs were seeded on a confluent layer for 24 h before the treatments were started. NAC (1 mM) was added to the culture mixture, which was incubated for 24 h.

DiI-Acetylated low-density lipoprotein (DiI-Ac-LDL) uptake and FITC-UEA-1 binding, tube formation and migration assays were performed[22–27,37,38,41–44]. Adherent cells were incubated with DiI-Ac-LDL (Life Technologies, Gaithersburg, MD, USA) and FITC-labeled Ulex Europaeus Agglutinin-I (Sigma, USA). The number of double-positive EPCs in each well was evaluated using a fluorescence microscope (Olympus, Tokyo, Japan). Three power fields were randomly counted.

A total of 4×10^4 EPCs at day 7 of culture were transferred to Matrigel-coated plates (Corning, NY, USA) and incubated for 48 h at 37 °C in 5% CO_2. Tube formation was measured by determining the relative tube length per field of view using an inverted light microscope. All cells in 3 random fields were counted

Cell migration was assayed using a transwell chamber (Corning, NY, USA). After 7 days of culture, the 4×10^4 EPCs were seeded in the upper chamber and cultured for 24 h. Cells on the bottom surface of the membrane stained with crystal violet were counted manually in 3 random fields/sample. Cell images were obtained on a phase-contrast microscope (Olympus, Tokyo, Japan).

Analysis of ROS levels, apoptosis rate and permeability

To detect intracellular ROS levels, cells were incubated with 10 μmol/l dichlorodihydrofluorescein diacetate (Beyotime, Beijing, China) at 37 °C for 15 min. The ROS levels were examined by flow cytometry and are expressed as the mean fluorescence intensity (MFI). To determine the apoptosis rate, the cells were incubated with Annexin-V and 7-amino-actinomycin D and then analyzed on a BD LSRFortessa (Becton Dickinson).

To evaluate the permeability of the BM EPCs, the cells were incubated with an antibody against CD144 (Abcam, Cambridge, MA) or ZO-1 (Abcam, Cambridge, MA) at 4 °C for another 30 min. The levels of CD144 and ZO-1 were analyzed using LSRFortessa software (Becton Dickinson) and are presented as the MFI (mean ± SEM).

HSCs were cocultured with BM EPCs

BM EPCs from patients with newly diagnosed AML or AML after CR and from HDs were cultured for 7 days. HSCs were isolated from HD BMMNCs using a CD34 MicroBead Kit (Miltenyi Biotec, Bergisch Gladbach, Germany) and cultured in noncontact culture with StemSpan™ SFEM (Stem Cell Technologies, Vancouver, BC, Canada). HSCs (1×10^5 per well) were cocultured with adherent BM EPCs(1×10^5 per well) for another 5 days, after which the nonadherent HSCs were collected for ROS level, apoptosis and CFUassays.

Primary leukemia cells, KG-1 cells or HL-60 cells were cocultured with BM EPCs

BM EPCs from patients with AML or CR and from HDs were cultured for 7 days. Primary leukemia cells were isolated from BMMNCs of newly diagnosed AML patients (N = 6) using a CD34 MicroBead Kit (Miltenyi Biotec, Bergisch Gladbach, Germany). KG-1 cells and HL-60 cells were obtained from the Cell Resource Center, Peking Union Medical College. Primary leukemia cells(1×10^5 per well), KG-1 cells(5×10^4 per well) or HL-60 cells(5×10^4 per well) were cultured in a noncontact culture system with BM EPCs(1×10^5 per well) in RPMI 1640 medium supplemented with 10% FBS and 1% penicillin/streptomycin for an additional 5 days. Then, nonadherent cells (primary leukemia cells, KG-1 cells or HL-60 cells) were collected for ROS level determination, apoptosis assay, 5-ethynyl-20-deoxyuridine (EdU) assay and CFU-L assay.

CFU and CFU-L assays

CFU or CFU-L were assayed using MethoCult™ H4434 Classic (Stem Cell Technologies). After 5 days of culture, 2×10^3 CD34$^+$ cells or 1×10^3 leukemia cells were plated in 24-well plates and cultured for 14 days. CFU-E, BFU-E, CFU-GM, and CFU-GEMM measurements were performed for CD34$^+$ cells. CFU-L measurements were performed for primary leukemia cells, KG-1 cells and HL-60 cells.

https://doi.org/10.1038/s41467-024-55051-x

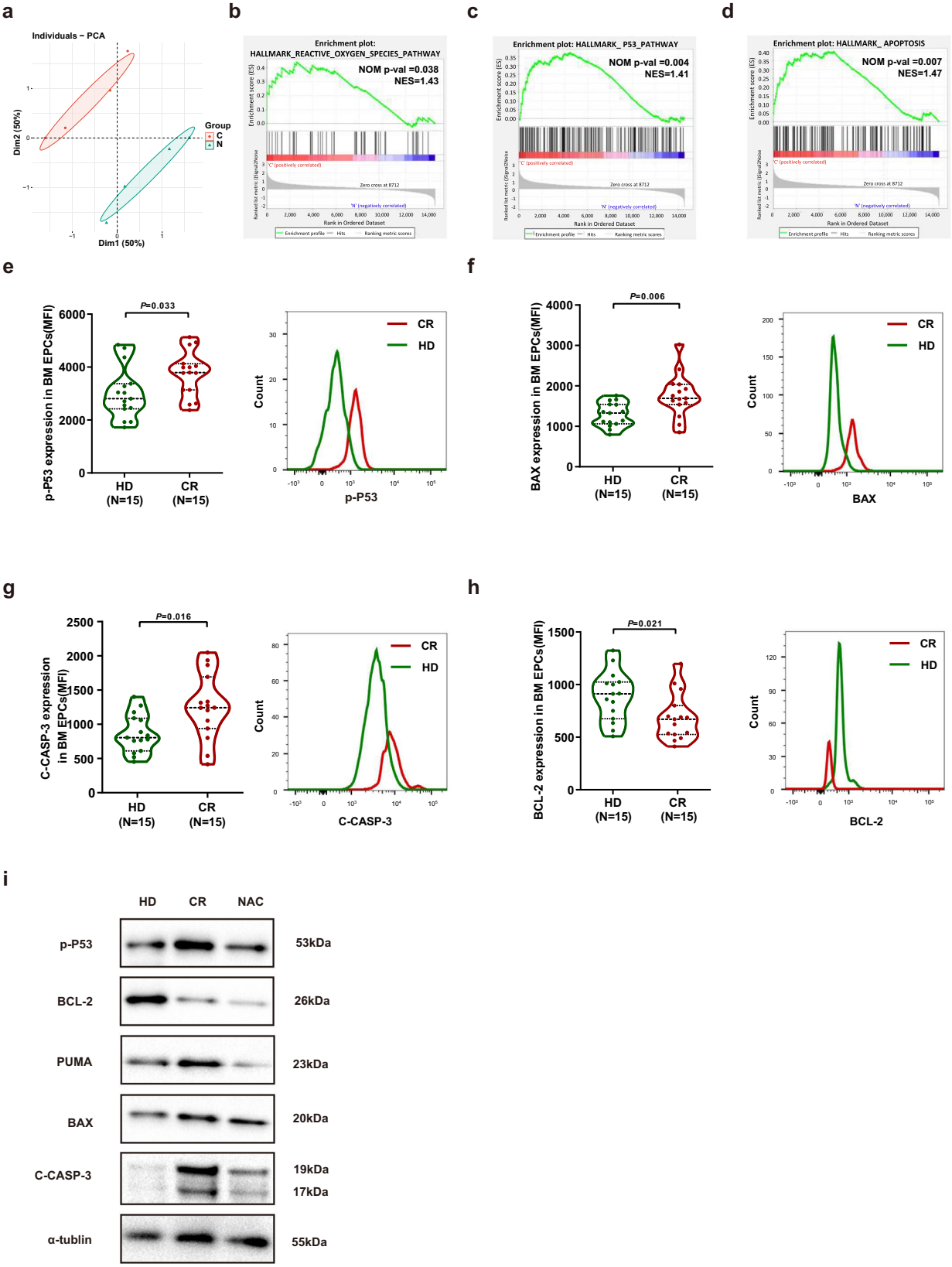

EdU assay

Primary leukemia cells, KG-1 cells and HL-60 cells were harvested after coculture with EPCs and were subsequently incubated with 50 μM EdU (RiboBio, China) in 48-well plates for 1 h at 37 °C. Then, according to the manufacturer's instructions, the nuclear fluorescence intensity was measured on a BD LSRFortessa (Becton Dickinson) and analyzed with BD LSRFortessa software (Becton Dickinson).

AML-ETO-induced AML mouse model and chemotherapy

GFP-expressing AML-ETO primary mouse AML cells were kindly provided by Professor Yue-Ying Wang of Rui-Jin Hospital, Shanghai Jiao

Fig. 5 | NAC improved the proliferation of BM EPCs from CR patients by inhibiting the ROS-p53 pathway. a PCA score plot of libraries of AML CR-EPCs treated with (N = 4) or without NAC (N = 4). The results of GSEA of differentially expressed genes in CR EPCs after CR and 7 days of culture treated with or without NAC, highlighting the inhibition of the **b** reactive oxygen species pathway, **c** P53 pathway and **d** apoptosis pathway. **a**–**d** Four paired samples from each of the groups (N = 4 per group, *n* = 1 per sample) were collected on different days, and analyzed on the same day. The intracellular levels of **e** phospho-p53 (p-P53), **f** BAX, **g** cleaved-caspase-3 (C-CASP-3), and **h** BCL-2 levels in HD EPCs (N = 15) or CR EPCs (N = 15) from BMMNCs were analyzed via flow cytometry (mean fluorescence intensity, mean ± standard error of the mean). **e**–**h** Fifteen paired samples from each of the groups (N = 15 per group, *n* = 1 per sample) were collected on different days, with one sample per group analyzed together on the same day. **i** Western blot analyses were performed on cultured HD EPCs or CR EPCs treated or not treated with NAC. The samples derived from the same gel for p-P53, BCL-2, PUMA, BAX, C-CASP-3 and α-tubulin were processed. All the western blot analyses were performed at least in triplicate, and representative images are shown. N represents biological replicates; n represents technical replicates. Statistical analyses were performed using the Mann–Whitney U test. The data are presented as the means ± SEMs.The statistical tests were two-sided and no adjustments were made for multiple comparisons. Source data are provided as a Source Data file.

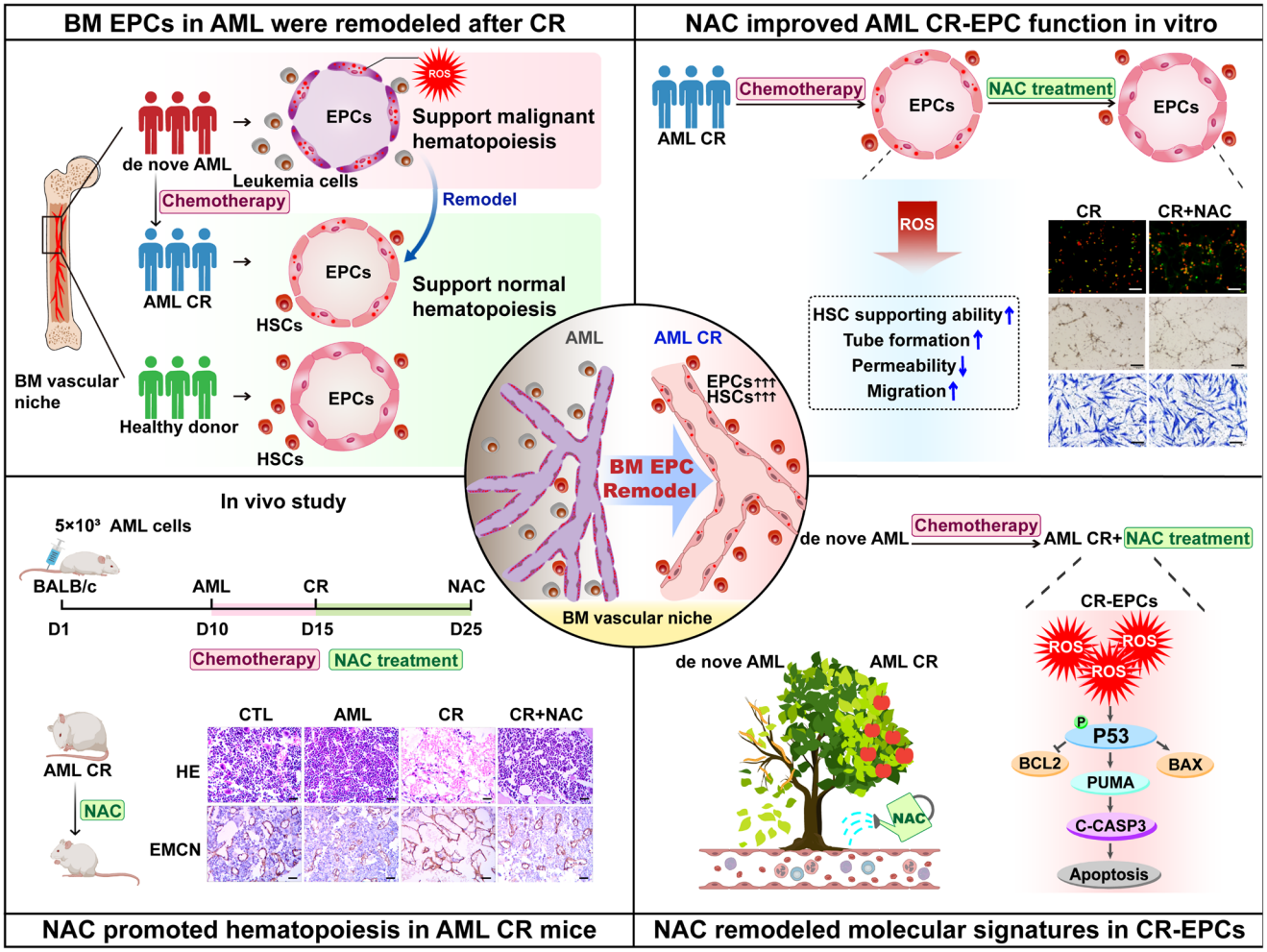

Fig. 6 | Schematic illustration of BM EPCs remodelling facilitates normal hematopoiesis during AML CR. Briefly, the function of BM EPCs in AML patients were remodeled to support normal hematopoiesis during CR. Experiments in vitro and in a classical AML murine and chemotherapy model confirmed that N-acetyl-L-cysteine(NAC, a ROS scavenging agent) can further facilitate normal hematopoiesis in AML after CR through enhancing CR-EPC function, providing a potential therapeutic strategy for AML patients after chemotherapy. Mechanistically, NAC remodeled molecular signatures in CR-EPCs and might enhance CR-EPC function via the ROS-P53 pathway.

Tong University School of Medicine[45]. The BALB/c female mice were purchased from the Beijing Vitalstar Biotechnology Co., Ltd. (Beijing China). All mice were housed in an environment of suitable temperature and humidity with ad libitum access to water and food (25 °C, suitable humidity (typically 50%), 12 h dark/light cycle). A total of 5×10^3 live GFP$^+$ AML-ETO leukemia cells were transplanted into non-irradiated recipient BALB/c female mice (6-8 weeks old) on day 0, leading to 20%-30% infiltration on day 10 and 80% BM infiltration on day 15.

AML burden in murine BM was estimated by regularly assessing the ratio of GFP$^+$ AML-ETO leukemia cells in peripheral blood by flow cytometry. AML bearing mice were ethically euthanized using carbon dioxide asphyxiation at indicated time points for sample collection or when the ratio of GFP$^+$ AML-ETO leukemia cells in murine BM reached to 80%, or 20% loss of original body weight.

To administer chemotherapy to AML mice, cytarabine (Ara-C) (100 mg/kg) was administered for 5 days, and doxorubicin (Doxo) (3 mg/kg) was injected intravenously for 3 days beginning on day 10. Ara-C was delivered with Doxo for the first 3 days and then alone for 2 days, mimicking the 7 + 3 regimen used for treating human AML patients[46].

For in vivo NAC treatment, mice were intraperitoneally injected with NAC (100 mg/kg/day; Sigma, St. Louis, MO) on days 15, 17, 19, 21,

23 and 25 (the NAC group). Simultaneously, the NAC-injected mice also received NAC in their drinking water from day 15 until the termination of the experiments. The untreated mice were given an equal volume of phosphate buffer solution at the same time.

All animal studies were approved by the Ethics Committee of Peking University People's Hospital (Protocol no. 2023PHE010).

RNA-seq and data analysis

RNA-seq analyses were performed to analyze AML EPCs (N = 4), CR EPCs (N = 4) and HD EPCs (N = 4) at day 7 of culture and cultivated BM EPCs from CR EPCs treated with NAC (N = 4) or not (N = 4) and paired HD EPCs (N = 4). Differentially expressed genes, principal component analysis, hierarchical clustering analysis, heatmap generation and volcano plotting construction were performed with the DESeq2, pheatmap, Volcano, clusterProfiler and ggplot2 packages in R (1.16.1). Gene set enrichment analysis was performed with respect to hallmark and C2 KEGG and C5 GO gene sets via GSEA software (version 4.3.2).

Intracellular protein detection by flow cytometry

Intracellular proteins were detected by flow cytometry according to previously described methods. Briefly, cells were incubated with EPC markers at 4 °C for 30 min and then fixed, permeabilized, and incubated with phospho-P53 (Abcam), BAX (BioLegend), BCL-2 (BioLegend) and cleaved-caspase-3 antibodies (Cell Signaling Technology). Intracellular protein levels were analyzed using LSRFortessa software (Becton Dickinson) and are expressed as the mean ± SEM (MFI).

Western blot analysis

Proteins were extracted from BM EPCs, and immunoblot analyses were performed with antibodies against phospho-P53 (Abcam), BCL-2 (Abcam), PUMA (Abcam), BAX (Abcam), cleaved-caspase-3 (Cell Signaling Technology), and α-tubulin (Sigma–Aldrich).

Statistics

Sample sizes were not predetermined by statistical methods. Investigators were not blinded to allocation during experiments and outcome assessment. SPSS 22.0 (SPSS, Chicago, IL), R version 4.2.2 (R Core Team, Vienna, Austria) and GraphPad Prism 8 (GraphPad Software, Inc., La Jolla, CA) were used for analysis. Mann–Whitney U test was used for continuous variables, paired *t* tests were performed to analyze the matched or paired data and unpaired *t* tests were performedin independent groups. *P*-values < 0.05 were considered to indicate statistical significance.

Reporting summary

Further information on research design is available in the Nature Portfolio Reporting Summary linked to this article.

Data availability

The raw sequence data generated in this study have been deposited in the Genome Sequence Archive for Human (GSA-Human) in National Genomics Data Center, China National Center for Bioinformation/Beijing Institute of Genomics, Chinese Academy of Sciences (GSA-Human: HRA006849) that are publicly accessible at https://ngdc.cncb.ac.cn/gsa-human/browse/HRA006849. Source data are provided with this paper.

References

1. Laurenti, E. & Göttgens, B. From haematopoietic stem cells to complex differentiation landscapes. *Nature* **553**, 418–426 (2018).
2. Crane, G. M., Jeffery, E. & Morrison, S. J. Adult haematopoietic stem cell niches. *Nat. Rev. Immunol.* **17**, 573–590 (2017).
3. Morrison, S. J. & Scadden, D. T. The bone marrow niche for haematopoietic stem cells. *Nature* **505**, 327–334 (2014).
4. Pinho, S. & Frenette, P. S. Haematopoietic stem cell activity and interactions with the niche. *Nat. Rev. Mol. Cell Biol.* **20**, 303–320 (2019).
5. Ding, L., Saunders, T. L., Enikolopov, G. & Morrison, S. J. Endothelial and perivascular cells maintain haematopoietic stem cells. *Nature* **481**, 457–462 (2012).
6. Zhao, H. Y. et al. M2 macrophages, but not M1 macrophages, support megakaryopoiesis by upregulating PI3K-AKT pathway activity. *Signal Transduct. Target Ther.* **6**, 234 (2021).
7. DiNardo, C. D., Erba, H. P., Freeman, S. D. & Wei, A. H. Acute myeloid leukaemia. *Lancet* **401**, 2073–2086 (2023).
8. Döhner, H., Weisdorf, D. J. & Bloomfield, C. D. Acute myeloid leukemia. *N. Engl. J. Med* **373**, 1136–1152 (2015).
9. Sipkins, D. A. et al. In vivo imaging of specialized bone marrow endothelial microdomains for tumour engraftment. *Nature* **435**, 969–973 (2005).
10. Hawkins, E. D. et al. T-cell acute leukaemia exhibits dynamic interactions with bone marrow microenvironments. *Nature* **538**, 518–522 (2016).
11. Doan, P. L. & Chute, J. P. The vascular niche: home for normal and malignant hematopoietic stem cells. *Leukemia* **26**, 54–62 (2012).
12. Medyouf, H. The microenvironment in human myeloid malignancies: emerging concepts and therapeutic implications. *Blood* **129**, 1617–1626 (2017).
13. Méndez-Ferrer, S. et al. Bone marrow niches in haematological malignancies. *Nat. Rev. Cancer* **20**, 285–298 (2020).
14. Shirzad, R. et al. Signaling and molecular basis of bone marrow niche angiogenesis in leukemia. *Clin. Transl. Oncol.* **18**, 957–971 (2016).
15. Newell, L. F. & Cook, R. J. Advances in acute myeloid leukemia. *BMJ* **375**, n2026 (2021).
16. Yang, X. & Wang, J. Precision therapy for acute myeloid leukemia. *J. Hematol. Oncol.* **11**, 3 (2018).
17. Bhansali, R. S., Pratz, K. W. & Lai, C. Recent advances in targeted therapies in acute myeloid leukemia. *J. Hematol. Oncol.* **16**, 29 (2023).
18. Bosshard, R., O'Reilly, K., Ralston, S., Chadda, S. & Cork, D. Systematic reviews of economic burden and health-related quality of life in patients with acute myeloid leukemia. *Cancer Treat. Rev.* **69**, 224–232 (2018).
19. Sauerer, T., Velázquez, G. F. & Schmid, C. Relapse of acute myeloid leukemia after allogeneic stem cell transplantation: immune escape mechanisms and current implications for therapy. *Mol. Cancer* **22**, 180 (2023).
20. Saluja, S., Bansal, I., Bhardwaj, R., Beg, M. S. & Palanichamy, J. K. Inflammation as a driver of hematological malignancies. *Front Oncol.* **14**, 1347402 (2024).
21. Chen, Q. et al. Apelin (+) Endothelial Niche Cells Control Hematopoiesis and Mediate Vascular Regeneration after Myeloablative Injury. *Cell Stem Cell* **25**, 768–783.e766 (2019).
22. Shi, M. M. et al. Atorvastatin enhances endothelial cell function in posttransplant poor graft function. *Blood* **128**, 2988–2999 (2016).
23. Kong, Y. et al. N-acetyl-L-cysteine improves bone marrow endothelial progenitor cells in prolonged isolated thrombocytopenia patients post allogeneic hematopoietic stem cell transplantation. *Am. J. Hematol.* **93**, 931–942 (2018).
24. Kong, Y. et al. Atorvastatin enhances bone marrow endothelial cell function in corticosteroid-resistant immune thrombocytopenia patients. *Blood* **131**, 1219–1233 (2018).
25. Tang, S. Q. et al. Repair of dysfunctional bone marrow endothelial cells alleviates aplastic anemia. *Sci. China Life Sci.* **66**, 2553–2570 (2023).
26. Kong, Y. et al. Prophylactic oral NAC reduced poor hematopoietic reconstitution by improving endothelial cells after haploidentical transplantation. *Blood Adv.* **3**, 1303–1317 (2019).

27. Wang, Y. et al. Prophylactic NAC promoted hematopoietic reconstitution by improving endothelial cells after haploidentical HSCT: a phase 3, open-label randomized trial. *BMC Med* **20**, 140 (2022).
28. Duarte, D. et al. Inhibition of endosteal vascular niche remodeling rescues hematopoietic stem cell loss in AML. *Cell Stem Cell* **22**, 64–77.e66 (2018).
29. Akinduro, O. et al. Proliferation dynamics of acute myeloid leukaemia and haematopoietic progenitors competing for bone marrow space. *Nat. Commun.* **9**, 519 (2018).
30. Cogle, C. R. et al. Functional integration of acute myeloid leukemia into the vascular niche. *Leukemia* **28**, 1978–1987 (2014).
31. Kumar, B. et al. Acute myeloid leukemia transforms the bone marrow niche into a leukemia-permissive microenvironment through exosome secretion. *Leukemia* **32**, 575–587 (2018).
32. Comazzetto, S., Shen, B. & Morrison, S. J. Niches that regulate stem cells and hematopoiesis in adult bone marrow. *Dev. Cell* **56**, 1848–1860 (2021).
33. Passaro, D. et al. Increased vascular permeability in the bone marrow microenvironment contributes to disease progression and drug response in acute myeloid leukemia. *Cancer Cell* **32**, 324–341.e326 (2017).
34. Yao, Y., Li, F., Huang, J., Jin, J. & Wang, H. Leukemia stem cell-bone marrow microenvironment interplay in acute myeloid leukemia development. *Exp. Hematol. Oncol.* **10**, 39 (2021).
35. Zahiragic, L. et al. Bevacizumab reduces VEGF expression in patients with relapsed and refractory acute myeloid leukemia without clinical antileukemic activity. *Leukemia* **21**, 1310–1312 (2007).
36. Fiedler, W. et al. A phase 2 clinical study of SU5416 in patients with refractory acute myeloid leukemia. *Blood* **102**, 2763–2767 (2003).
37. Kong, Y. et al. Association of an impaired bone marrow microenvironment with secondary poor graft function after allogeneic hematopoietic stem cell transplantation. *Biol. Blood Marrow Transpl.* **19**, 1465–1473 (2013).
38. Kong, Y. Poor graft function after allogeneic hematopoietic stem cell transplantation-an old complication with new insights(☆). *Semin Hematol.* **56**, 215–220 (2019).
39. Baryawno, N. et al. A cellular taxonomy of the bone marrow stroma in homeostasis and leukemia. *Cell* **177**, 1915–1932 e1916 (2019).
40. Döhner, H. et al. Diagnosis and management of AML in adults: 2022 recommendations from an international expert panel on behalf of the ELN. *Blood* **140**, 1345–1377 (2022).
41. Lyu, Z. S. et al. The glycolytic enzyme PFKFB3 determines bone marrow endothelial progenitor cell damage after chemotherapy and irradiation. *Haematologica* **107**, 2365–2380 (2022).
42. Lyu, Z. S. et al. Autophagy in endothelial cells regulates their haematopoiesis-supporting ability. *EBioMedicine* **53**, 102677 (2020).
43. Xing, T. et al. Dysfunctional bone marrow endothelial progenitor cells are involved in patients with myelodysplastic syndromes. *J. Transl. Med.* **20**, 144 (2022).
44. Liang, M. et al. Activation of PPARδ in bone marrow endothelial progenitor cells improves their hematopoiesis-supporting ability after myelosuppressive injury. *Cancer Lett.* **592**, 216937 (2024).
45. Wang, Y. Y. et al. C-KIT mutation cooperates with full-length AML1-ETO to induce acute myeloid leukemia in mice. *Proc. Natl Acad. Sci. USA* **108**, 2450–2455 (2011).
46. Guo, H. Z. et al. Leukemic progenitor cells enable immunosuppression and post-chemotherapy relapse via IL-36-inflammatory monocyte axis. *Sci. Adv.* **7**, eabg4167 (2021).

Acknowledgements

This work was supported by the National Key R&D Program of China (2022YFA1103300, 2021YFA1100900), the National Natural Science Foundation of China (82270229, 82070188), Major Program of the National Natural Science Foundation of China (82293630), Beijing Natural Science Foundation (7232181). The authors thank all of the core facilities at the Peking University Institute of Hematology for patient care and sample collection, thank HTL and ML for excellent assistance with drawing the schematic illustration image. American Journal Experts (www.journalexperts.com) provided editorial assistance to the authors during the preparation of the manuscript.

Author contributions

X.J.H. and Y.K.: Conceptualization, Funding acquisition, Project administration, Supervision, Writing - review & editing the manuscript. T.X., and L.J.H.: Data curation, Investigation, Methodology, Writing and revising the manuscript; H.Y.Z., C.Y.L., Z.K.W., M.Z.S., and Z.S.L.: Data curation, Investigation, and revising the manuscript. J.W., Y.W., H.J., Q.J., Y.J.C., X.H.Z.: Resources and clinical sample collection.

Competing interests

The authors declare no competing interests.

Additional information

Supplementary information The online version contains supplementary material available at https://doi.org/10.1038/s41467-024-55051-x.

Correspondence and requests for materials should be addressed to Yuan Kong or Xiao-Jun Huang.

Peer review information *Nature Communications* thanks the anonymous reviewers for their contribution to the peer review of this work. A peer review file is available.

Reprints and permissions information is available at http://www.nature.com/reprints

Publisher's note Springer Nature remains neutral with regard to jurisdictional claims in published maps and institutional affiliations.

Open Access This article is licensed under a Creative Commons Attribution-NonCommercial-NoDerivatives 4.0 International License, which permits any non-commercial use, sharing, distribution and reproduction in any medium or format, as long as you give appropriate credit to the original author(s) and the source, provide a link to the Creative Commons licence, and indicate if you modified the licensed material. You do not have permission under this licence to share adapted material derived from this article or parts of it. The images or other third party material in this article are included in the article's Creative Commons licence, unless indicated otherwise in a credit line to the material. If material is not included in the article's Creative Commons licence and your intended use is not permitted by statutory regulation or exceeds the permitted use, you will need to obtain permission directly from the copyright holder. To view a copy of this licence, visit http://creativecommons.org/licenses/by-nc-nd/4.0/.

© The Author(s) 2024